Nano Energy 60 (2019) 324–331

Contents lists available at ScienceDirect

Nano Energy

journal homepage: www.elsevier.com/locate/nanoen

Full paper

Ideal conducting polymer anode for perovskite light-emitting diodes by molecular interaction decoupling

Su-Hun Jeong[a], Hobeom Kim[a], Min-Ho Park[a], Yeongjun Lee[a], Nannan Li[b], Hong-Kyu Seo[c], Tae-Hee Han[a], Soyeong Ahn[b], Jung-Min Heo[a], Kwang S. Kim[b], Tae-Woo Lee[a,d,*]

[a] Department of Materials Science and Engineering, Seoul National University, 1 Gwanak-ro, Gwanak-gu, Seoul, 08826, Republic of Korea
[b] Department of Chemistry, Center for Superfunctional Materials, Ulsan National Institute of Science and Technology (UNIST), Ulsan, 44919, South Korea
[c] Department of Materials Science and Engineering, Pohang University of Science and Technology (POSTECH), Pohang, Gyeongbuk, 790-784, Republic of Korea
[d] Research Institute of Advanced Materials, BK21 PLUS SNU Materials Division for Educating Creative Global Leaders, Nano System Institute (NSI), Institute of Engineering Research, Research Institute of Advanced Materials, Seoul National University, 1 Gwanak-ro, Gwanak-gu, Seoul, 08826, Republic of Korea

ARTICLE INFO

Keywords:
Metal halide perovskite
Perovskite light emitting diodes
Polycrystalline perovskite film
Conducting polymer anode

ABSTRACT

An ideal conducting polymer anode (CPA) in organic and perovskite light-emitting diodes (LEDs) requires high electrical conductivity κ, high work function *WF*, and prevention of exciton quenching between an anode and an overlying emitting layer. However, increasing the κ and *WF* at the same time has been a very challenging unsolved issue due to their trade-off relationship: previous approaches to increase the *WF* have reduced the films' κ and vice versa. Therefore, delicate molecular scale control of the conducting polymer compositions are required to solve this fundamental issue. Here, we introduce an effective molecular scale control strategy to decouple the *WF* with κ in a CPA while maintaining blocking capability of exciton quenching. This change resulted in a high current efficiency up to 52.86 cd A^{-1} (10.93% ph el^{-1}) in green polycrystalline perovskite LEDs. Our results provide a significant clue to develop effective CPAs for highly-efficient organic and perovskite LEDs.

1. Introduction

Organic and perovskite optoelectronic devices including solar cells and light-emitting diodes [1–3] require at least one transparent electrode to allow light to penetrate for applications to solar energy panels, solid-state lightings, and panel displays; flexible devices further require flexible transparent electrodes. Indium tin oxide (ITO) anode is not only brittle but also detrimental to perovskite light-emitting diodes (PeLEDs) because the In and Sn species can be migrated from the ITO anode and acts as a charge-trapping or luminescence quenching center in the devices [4]. Conducting polymers are good candidates to avoid the issue of the ITO and realize flexible devices. The most widely-used conducting polymer is poly(3,4-ethylenedioxythiophene):poly(4-styrenesulfonate) (PEDOT:PSS) (Fig. 1a and b); it is also flexible, and it has possible applications in stretchable electronic devices [5–8]. Recently, highly-efficient organic light-emitting diodes (OLEDs) and PeLEDs with a simple structure without a hole injection layer have been fabricated using a modified PEDOT:PSS anode which has high work function *WF* even though some electrical conductivity κ was sacrificed [9]. Until now, chemical or molecular approaches to increase the *WF* in conducting polymer compositions have reduced the films' κ and vice versa [4,10–14]. Achieving high κ and high *WF* simultaneously is very challenging, especially to realize highly-efficient simplified OLEDs and PeLEDs without a hole injection layer that operate at low voltage because the organic or perovskite emitting layer with a deep-lying valence band maximum (VBM) level gives a high hole injection barrier from the conventional anode.

Conventional methods to increase the κ of conducting polymers to be used in electrodes can be classified into two categories: (i) addition of polar organic solvent additives (e.g. dimethyl sulfoxide (DMSO), ethylene glycol) to control the morphology of conducting polymers [15–18], and (ii) chemical post-treatment with solvents and liquid acids to remove extra PSS [19–26]. All these post-treatments entail an additional step and the processes are not suitable for mass production with reliable control of the film.

Previously-reported methods to increase κ in PEDOT:PSS always reduce *WF*, and the resulting high-κ conducting polymer films provide severe exciton quenching pathway between the anode and the overlying emitting layer. These traits of the films severely reduce their usability as anodes for simplified OLEDs and PeLEDs. The reported post-treatment methods after formation of PEDOT:PSS films decrease the surface *WF* by intentionally removing insulating PSS chains [21]. The

* Corresponding author. Department of Materials Science and Engineering, Seoul National University, 1 Gwanak-ro, Gwanak-gu, Seoul, 08826, Republic of Korea.
E-mail addresses: twlees@snu.ac.kr, taewlees@gmail.com (T.-W. Lee).

https://doi.org/10.1016/j.nanoen.2019.03.030
Received 6 December 2018; Received in revised form 24 February 2019; Accepted 7 March 2019
Available online 12 March 2019
2211-2855/

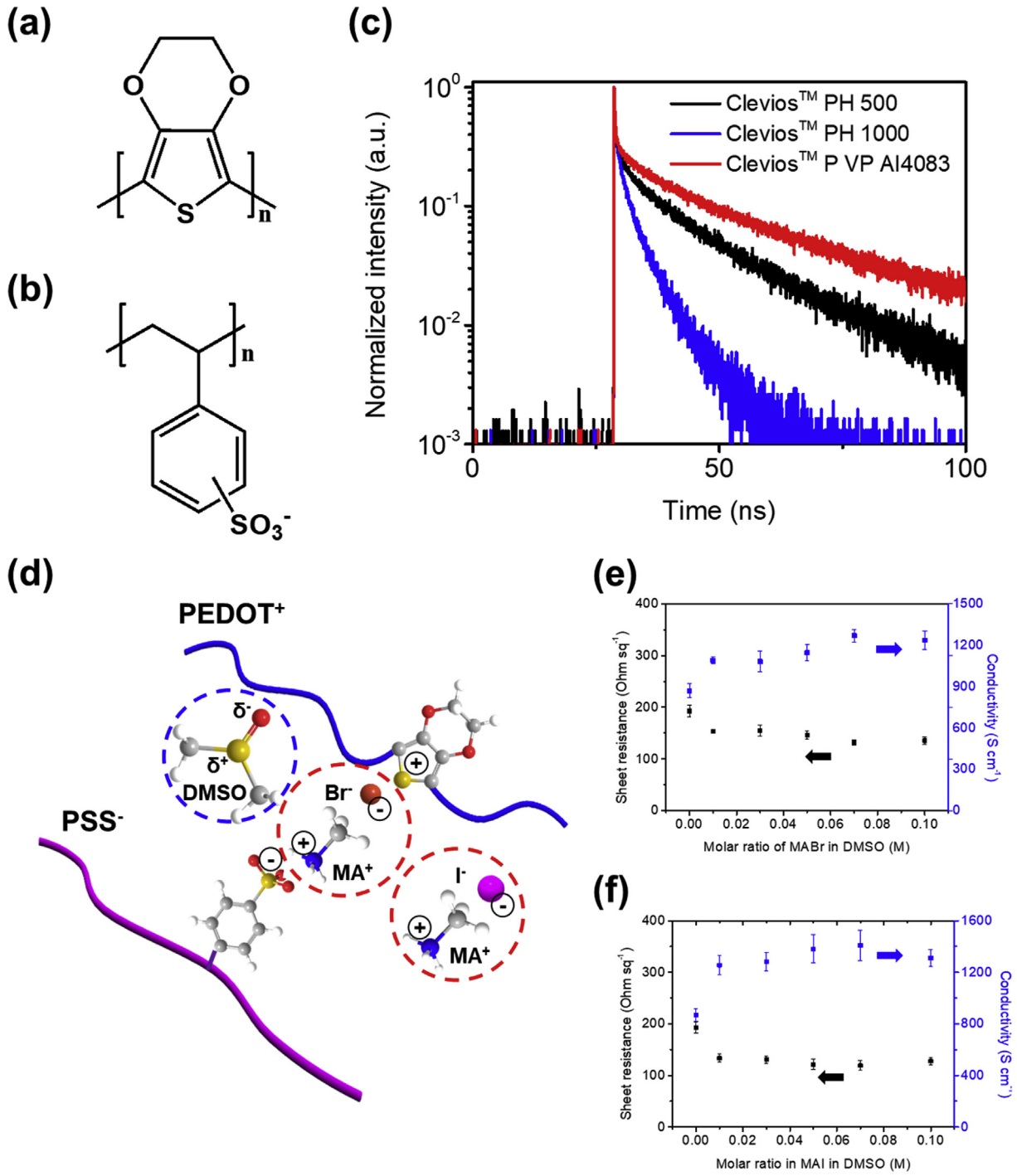

Fig. 1. Chemical structure of (a) PEDOT and (b) PSS^-. (c) PL lifetime curves of $MAPbBr_3$ layers on top of various PEDOT:PSS films. (d) Schematic illustration of weakening of Coulombic interaction between PEDOT and PSS by DMSO, MABr, and MAI additives. Sheet resistance and conductivity of PEDOT:PSS films with varying ratios of (e) MABr and (f) MAI in DMSO.

decreased *WF* is too low to make ohmic contact with overlying organic emitter (usually the highest occupied molecular orbital > 5.5 eV) and metal halide perovskite (MHP) layers (VBM level ~5.9 eV for methylammonium lead bromide ($MAPbBr_3$) [11], so to achieve devices that have high efficiency, additional hole injection layers are required [27–30].

Exciton quenching between anodes and MHP layers by conventional PEDOT:PSS also seriously impedes use of PEDOT:PSS especially in anodes of polycrystalline PeLEDs in which the polycrystalline MHP with grains > 100 nm has fundamental limitations of a long exciton diffusion length (> 100 nm) and low exciton binding energy unlike quasi-2D and quantum dots or nanoparticles < 20 nm [14,31–33]. Compared to organic emitting materials, polycrystalline MHPs have low exciton binding energy (76 or 150 meV for $MAPbBr_3$) [34], so diffusing excitons can be easily quenched between metallic PEDOT:PSS and MHP layers. Therefore, overcoming the trade-off relationship among parameters (i.e. *WF*, κ, and ability to prevent exciton quenching) especially by decoupling the *WF and exciton-quenching-blocking capability* with the κ is a difficult task. Therefore, an effective conducting polymer material system must be developed to overcome those

problems.

In this work, we developed a systematic molecular scale decoupling strategy to realize an ideal conducting polymer anode (CPA) for organic and perovskite LEDs; this CPA has high κ ($> 1400\,S\,cm^{-1}$), high *WF* (~ 5.85 eV), and good ability to prevent exciton quenching. For conducting polymers, we developed effective co-additives composed of alkylammonium halides, polar solvent, and perfluorinated ionomer (PFI) to increase those three parameters simultaneously. The addition of fluoropolymer in the CPA composition increases *WF* and enhances exciton-quenching blocking capability in the devices and but reduces the κ of the CPA. The alkylammonium halides were added to increase the κ of the conducting polymer compositions with a PFI, while they do not change the *WF* of the compositions. We used Raman spectroscopy, time-resolved photoluminescence, density functional theory calculation and softness parameter analysis to understand this synergetic simultaneous improvement of the *WF*, κ and exciton-quenching-blocking capability. The alkylammonium halides additives in the PEDOT:PSS:PFI-based CPAs were used to weaken the coulombic interaction between PEDOT and PSS, decouple the *WF* with the κ, and thereby to increase the κ due to improved interaction of conducting PEDOT domains. We suggest that this approach is effectively used to achieve a high current efficiency up to 52.86 cd A^{-1} (10.93% ph el^{-1}) in green polycrystalline perovskite LEDs.

2. Experimental section

2.1. Preparation of conducting polymer films

Various molar ratios of methyl ammonium bromide (MABr)/DMSO or methyl ammonium iodide (MAI)/DMSO were added to PEDOT:PSS (Clevios™ PH 1000). The solution was purified by passing it through a filter (0.45-μm pore size, Whatman), then spin-coated at 1000 rpm for 90 s. The resulting films were annealed at 200 °C for 10 min.

2.2. Film characterization (atomic force microscope (AFM)/Raman spectroscopy/XRD/Kelvin probe)

The surface morphologies of PEDOT:PSS films were measured using an AFM (NanoScope® IIIa, Digital Instruments). The Raman spectra of PEDOT:PSS films were measured using an Raman spectroscopy (Renishaw co.) equipped with a 633-nm diode laser. The XRD patterns of PEDOT:PSS films were obtained by using a Rigaku D/max-2500 diffractometer (with Cu-*K*α radiation ($\lambda = 1.540593$ Å) at 40 kV and 100 mA). The *WF* of PEDOT:PSS films was measured using a Kelvin probe (SKP-5050, KP technology).

2.3. Fabrication of PeLEDs

We also added PFI (Sigma Aldrich) as a *WF*-tuning material, because PFI has high ionization potential. Then 80-nm-thick anode films with the different additives were fabricated using spin-coating, then annealed at 200 °C for 10 min in air. The films were moved to a nitrogen glove box and $MAPbBr_3$ solution was spin-coated on them at 3000 rpm for 60 s. During spin-coating, a nanocrystal pinning process using 2,2′,2″-(1,3,5-benzinetriyl)-tris(1-phenyl-1-H-benzimidazole) (TPBi) in chloroform [11] was used. The samples were annealed at 90 °C for 10 min. A 50-nm-thick TPBi layer was deposited as an electron-transporting layer by using a high-vacuum thermal evaporator ($< 5 \times 10^{-7}$ Torr), then LiF (1 nm)/Al (100 nm) were sequentially deposited as cathode layers. Fabricated PeLEDs were encapsulated with a glass lid by using an epoxy resin in a nitrogen glove box.

2.4. I–V-L characterization of PeLEDs

The I–V–L characteristics were measured using a Keithley 236 source measurement unit and a Minolta CS2000 spectroradiometer.

3. Results and discussion

First, we quantified how PSS concentration affects exciton-quenching in glass/PEDOT:PSS (Clevios™ P VP AI4083, PH 500 or PH 1000)/$MAPbBr_3$ films. We measured the photoluminescence (PL) lifetime (Fig. 1c) of $MAPbBr_3$ layers on top of various commercially-available PEDOT:PSS films (Table S1). $MAPbBr_3$ layers on top of high-κ PEDOT:PSS (Clevios™ PH 500, PH 1000) for electrodes showed much shorter PL lifetime than did $MAPbBr_3$ layers on low-κ PEDOT:PSS (Clevios™ P VP AI4083, $10^{-3} - 10^{-4}\,S\,cm^{-1}$) with high ratio of PSS to PEDOT which has been commonly used for a hole injection layer (Fig. 1c; Table S2).

The short PL lifetime of $MAPbBr_3$ layers on top of PEDOT:PSS is a result of the lack of PSS chains on the surface of the PEDOT:PSS film. PSS chains are electrically insulating and therefore prevent charge transfer between PEDOT chains; to reduce this effect, PEDOT:PSS for electrodes (Clevios™ PH 500, PH 1000) has a low ratio of PSS to PEDOT. In contrast, the PEDOT:PSS used for hole-injection layers (Clevios™ P VP AI4083) has a high ratio of PSS to PEDOT, to increase the *WF* (Table S1) [35]. The surface of PEDOT:PSS films was enriched in insulating PSS chains, which have wide energy band gap and therefore block electrons at the interface between anodes and overlying semiconducting layers; as a result, recombination of electrons at the anodes is impeded (Fig. S1). Therefore, the lack of PSS chains causes direct contact between metallic PEDOT chains and semiconducting layers, and as a result, causes severe exciton dissociation.

We introduced two new co-additives composed of a PFI and an alkylammonium halide, which increased κ to $> 1400\,S\,cm^{-1}$ without any damage to PEDOT:PSS films and the *WF* to make a high-*WF* polymeric anode (HWFPA) composed of PEDOT, PSS, and PFI. The PFI also take a role to effectively prevent exciton quenching between the polymeric anode and the overlying emitting layer.

We used aqueous solution of PEDOT:PSS (Clevios™ PH 1000), which can give a high κ and is widely used in electrodes. To it, we added 5 wt % of solutions with various molar ratios of MABr or MAI in DMSO (Fig. 1d). PEDOT:PSS film with only-DMSO additive showed $\kappa = 868.31 \pm 51.08\,S\,cm^{-1}$; when 0.07 M MABr was added, the film had $\kappa = 1269.81 \pm 45.69\,S\,cm^{-1}$, and when 0.07 M MAI was added, the film had $\kappa = 1408.47 \pm 116.77\,S\,cm^{-1}$ (Fig. 1e and f; Tables S3 and S4), which is the highest κ yet achieved using only chemical additives without post-treatment (Fig. S2; Table S5). Regardless of the additives, the PEDOT:PSS films showed similar high transmittance in the entire visible range (Fig. S3); this result implies that the additives did not affect the film thickness after spin-coating at the same speed. In the X-ray photoelectron spectra (XPS), the S(2p) peaks were at binding energies of 167.69 and 163.9 eV, which correspond to the sulfur from the sulfonate and thiophene of PSS and PEDOT, respectively (Fig. S4) [21]. The S(2p) peaks were not affected by the MAI/DMSO or MABr/DMSO additives; this result means that these additives did not affect the ratio of PSS to PEDOT.

To identify the effect of MAI/DMSO or MABr/DMSO additive, we used an AFM to visualize the changes in surface morphology of PEDOT:PSS films after the addition of DMSO, MAI/DMSO or MABr/DMSO (Fig. 2). In AFM force modulation images (Fig. 2e–h), bright regions indicate PEDOT-rich grains, and dark regions indicate PSS-rich grains [36]. The pristine PEDOT:PSS films showed disconnected conducting PEDOT-rich grains; this morphology indicates weak phase separation between PEDOT and PSS chains. In contrast, the PEDOT:PSS films with DMSO or MABr/DMSO had granular domains and better connections between PEDOT-rich grains than pristine PEDOT:PSS films did (Fig. 2f and g). Especially, the film with MAI/DMSO showed a long, stretched network of PEDOT-rich grains like nanofibrils (Fig. 2h).

To investigate the crystallinity of PEDOT chains after adding the MABr/DMSO or MAI/DMSO, we performed x-ray diffraction (XRD) measurement (Fig. 3a). PEDOT:PSS films with added MABr/DMSO or MAI/DMSO showed larger and sharper XRD peaks than the pristine

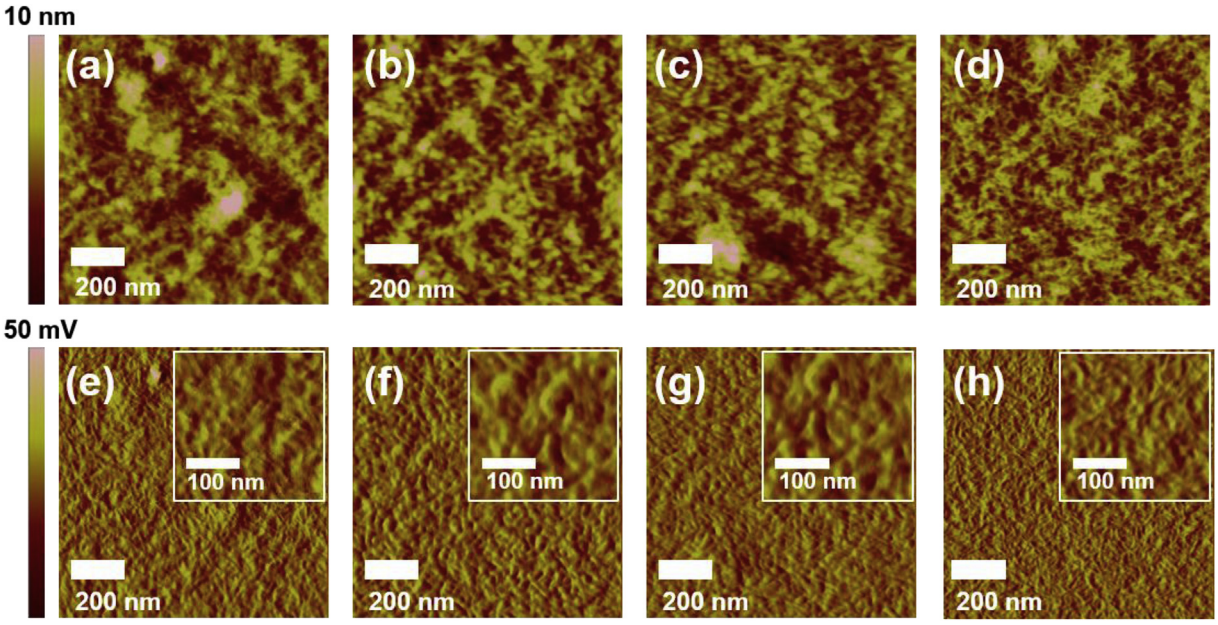

Fig. 2. AFM surface images of PEDOT:PSS films. (a, e) Pristine, (b, f) DMSO, (c, g) 0.07 M MABr/DMSO, and (d, h) 0.07 M MAI/DMSO-added PEDOT:PSS films. a, b, c and d are height images; e, f, g and h are force modulation images.

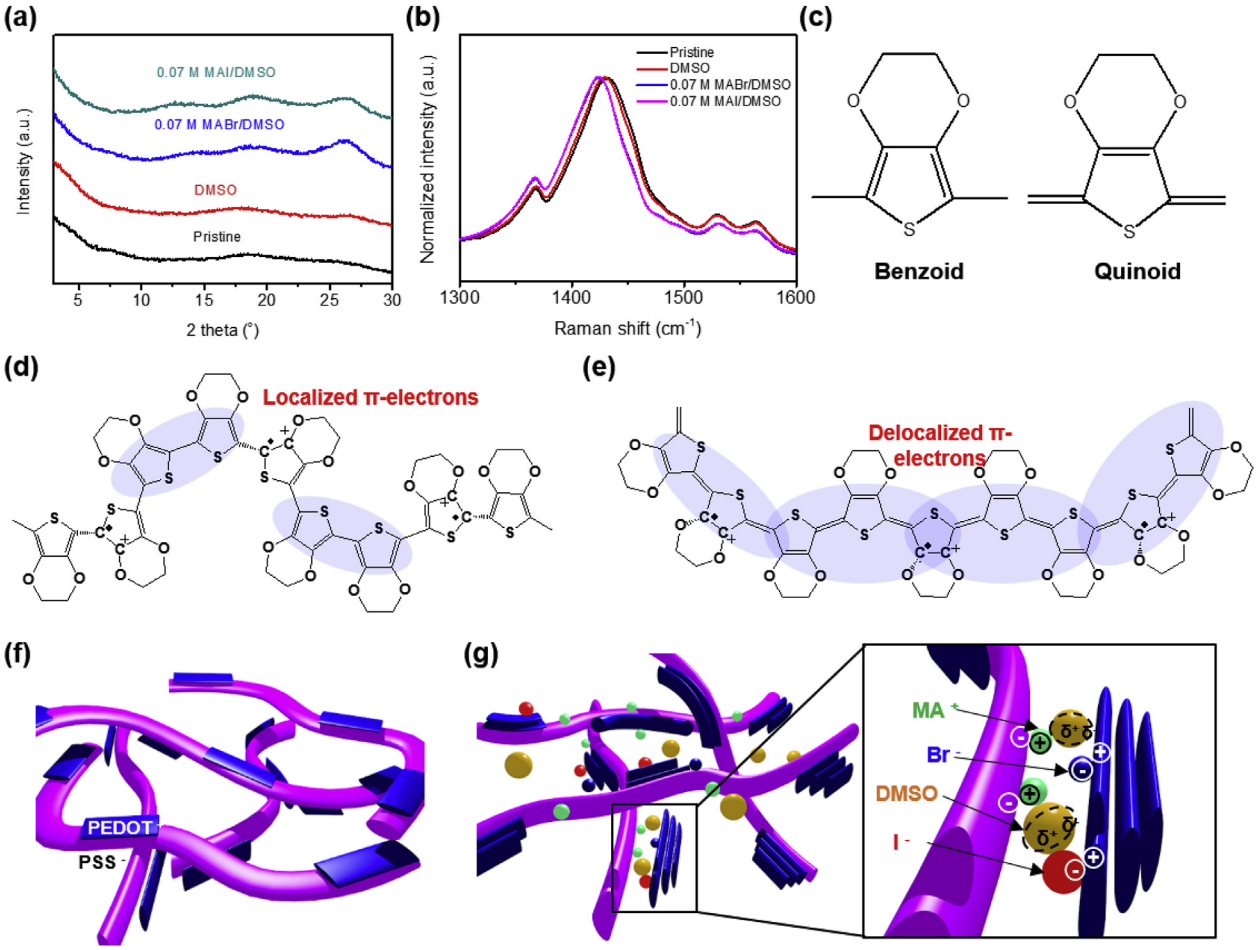

Fig. 3. (a) XRD patterns and (b) Raman spectra of the four types of PEDOT:PSS film. (c) Two resonance structures of thiophene rings in PEDOT chains. (d) Localized π-electrons in PEDOT chain with coil conformation and (e) delocalized π-electrons in PEDOT chain with linear-like coil conformation. Schematic illustrations of $PEDOT^+$ and PSS^- chains (f) before and (g) after addition of alkylammonium halide/DMSO additives.

PEDOT:PSS film. Among the several peaks, the peak around 26° is a result of the π-π stacking of PEDOT chains [20,37]. After the addition of MABr/DMSO or MAI/DMSO, a large and sharp peak around 26° appeared, which is an indication of strengthened π-π stacking of thiophene rings in the PEDOT chains.

To determine at the molecular level why κ increases, Raman spectroscopy was performed. Raman spectra (Fig. 3b) were obtained for a pristine PEDOT:PSS film, and for PEDOT:PSS films amended with DMSO only, with MABr/DMSO, or with MAI/DMSO. The spectra differed between 1400 and 1500 cm^{-1}. As the κ of the PEDOT:PSS films increased, the peak values were red-shifted (1432.06 cm^{-1} for Pristine, 1428.43 cm^{-1} for DMSO, 1424.78 cm^{-1} for 0.07 M MABr/DMSO, and 1422.05 cm^{-1} for 0.07 M MAI/DMSO). This trend can be explained by the resonant structure transformations between the benzoid and quinoid structures of the thiophene ring on the PEDOT chains (Fig. 3c) [38,39]. When the quinoid resonant structure becomes dominant, the shoulder of the Raman spectrum at the low position disappears [40]. The transformation of the resonance structures of PEDOT chains is attributed to a conformational change of conjugated chains. Presumably, PEDOT chains can have coiled or linear conformations. After the addition of DMSO, MABr/DMSO or MAI/DMSO, the linear-like coiled conformations become dominant. In the coiled conformation, the neighboring thiophene ring planes on the PEDOT chains deviate (Fig. 3d), so the conjugated π-electrons are not sufficiently delocalized. However, in the linear conformation, the neighboring thiophene rings are coplanar so the π-electrons can be relatively delocalized (Fig. 3e). As a result, the quinoid structure is favored, so κ increases [41]. Therefore, the increase in κ after addition of MAI/DMSO or MABr/DMSO is a result of a weakened electrostatic interaction between PEDOT and PSS chains, and of improved π-π stacking of PEDOT chains (Fig. 3f and g).

The high dipole moment of DMSO caused by charge delocalization can effectively screen the Coulombic interaction between positive charged PEDOT and negative charged PSS chains [18]. The strong dipole-dipole or dipole-charge interaction between DMSO molecule and PEDOT:PSS chains causes formation of conducting PEDOT-rich domains by inducing phase separation between the PEDOT and PSS chains.

The additional effect of alkylammonium halides can be explained by using the softness parameter σ of ion species. σ is related to how well ion species can associate with other ion species. Especially, cations that have $\sigma > 0$ can strongly associate with the PSS^- chains, whereas anions that have $\sigma > 0$ can strongly associate with the $PEDOT^+$ chains [42,43]. MA^+ has $\sigma = +10.7$, Br^- has $\sigma = +0.17$ and I^- has $\sigma = +0.5$ [44]. Therefore, MA^+ can strongly interact with the PSS^- chains, and Br^- and I^- can strongly interact with $PEDOT^+$ chains. The MA^+, Br^- and I^- ions exert a screening effect that weakens the Coulombic interaction between the PSS^- and $PEDOT^+$ chains, so the PSS chains can aggregate and the PEDOT chains can separate.

To determine the electrostatic interaction between the ions, the molecular binding energy (ΔE) for each combination was calculated using density functional theory (DFT) (Fig. 4). ΔE between positively-charged PEDOT and negatively-charged PSS was $-306\ kJ\ mol^{-1}$ ($PEDOT^+$:PSS^-), while ΔE between MA cation and negatively-charged PSS was $-493\ kJ\ mol^{-1}$, indicating that the exchange of counter ions, $PEDOT^+$ and MA^+, is energetically favorable when MABr or MAI is added into PEDOT:PSS films. Furthermore, compared to MA^+:PSS^- combination ($\Delta E = -493\ kJ\ mol^{-1}$), MABr shows a slightly more negative binding energy value ($\Delta E = -500\ kJ\ mol^{-1}$) and contrarily MAI has a much lower binding energy ($\Delta E = -470\ kJ\ mol^{-1}$). Therefore, we expect that MAI can exchange much more counter ions with PEDOT:PSS than MABr to form the more stable combination MA^+:PSS^-. The binding energy calculation combined with the softness parameters analysis showed that methyl ammonium halides can selectively increase the molecular interaction of PEDOT domains separately from PSS. Therefore, effective decoupling of κ with *WF* can also be achieved to increase the κ and *WF* at the same time by separating the PEDOT domains from PFI chains.

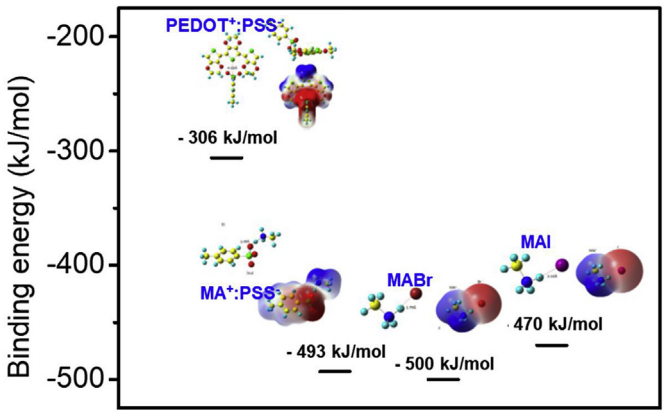

Fig. 4. Binding energy diagrams of various combinations of PEDOT:PSS and organic salts.

We first fabricated polymeric organic light-emitting diodes (PLEDs) on the high *WF* polymeric anodes (HWFPAs) that incorporate a PFI, tetrafluoroethylene-perfluoro-3,6-dioxa-4-methyl-7-octenesulfonic acid copolymer (Fig. S5) [9,11]. The addition of MABr or MAI resulted in an increase in the κ of the anode (Table S6), without affecting its *WF* (~5.85 eV) (Fig. S6). The device structure of PLED was HWFPA with 5 wt% of different solutions (80 nm)/green-emitting fluorene copolymer (Dow LUMANTION Green B, Dow Chemical Co.) (80 nm)/LiF (1 nm)/Al (100 nm) (Fig. S7a). As κ of the anodes increased, the current densities at the same voltages increased (Fig. S7b) and operating voltages at the same luminance decreased (Fig. S7c). Also, the current efficiencies *CEs* increased up to 11.53 cd A^{-1} for 0.01 M MAI/DMSO-added HWFPA-based PLED (9.70 cd A^{-1} for DMSO and 11.11 cd A^{-1} for 0.01 M MABr/DMSO) (Fig. S7d).

We used the reported structures of PeLEDs to quantify how the increased κ of our HWFPA affected the device characteristics [9,11]. The device structure was HWFPA with different solutions (DMSO-only, 0.01 M MABr/DMSO, or 0.01 M MABr/DMSO) (80 nm)/$MAPbBr_3$ (400 nm)/TPBi (50 nm)/LiF (1 nm)/Al (100 nm) (Fig. 5a). Maximum current efficiency CE_{max} was only 41.01 cd A^{-1} in the device that used HWFPA with added DMSO, but 51.82 cd A^{-1} in the device that used HWFPA with added MABr/DMSO, and 52.86 cd A^{-1} in the device that used HWFPA with added MAI/DMSO (Fig. 5b). As κ of the anodes increased, the current densities at the same voltages increased (Fig. 5c) and operating voltages at the same luminance decreased (Fig. 5d). The turn-on voltages of OLEDs and PeLEDs are mostly determined by the energy level offsets at charge injecting contacts. In our case, the difference in *WF* of anodes and VBM of overlying $MAPbBr_3$ would determine the turn-on voltages of devices. According to our previous results, as the σ of ions in the added organic salts increased, PEDOT and PSS chains could be more separated into each domain. The PSS-rich domains have higher *WF* [35], which facilitate hole injection through the PSS-rich domains and thus reduce the turn-on voltages. Therefore, the CPAs with MAI, which have the well-separated PEDOT-rich and PSS-rich domains, can have the lowest turn-on voltage. The electroluminescence (EL) spectrum of PeLEDs was very narrow, with a full width at half maximum of ~20 nm (Fig. 5e). The calculated maximum external quantum efficiencies (EQEs) were 8.54% ph el^{-1} in the HWFPA-based PeLED with only DMSO added, 10.63% ph el^{-1} in the device with DMSO and MABr, and 10.93% ph el^{-1} in the device with DMSO and MAI (Fig. 5f). We measured the EL degradation of our devices during operation (Fig. S8). The initial luminance of all devices was fixed at 100 cd m^{-2}, and the measurement was conducted until the initial luminance decreased to half. As MABr and MAI were additionally added, the overshoot, which means the rapid increase in luminance at the early stage of lifetime measurement, decreased, and the half-

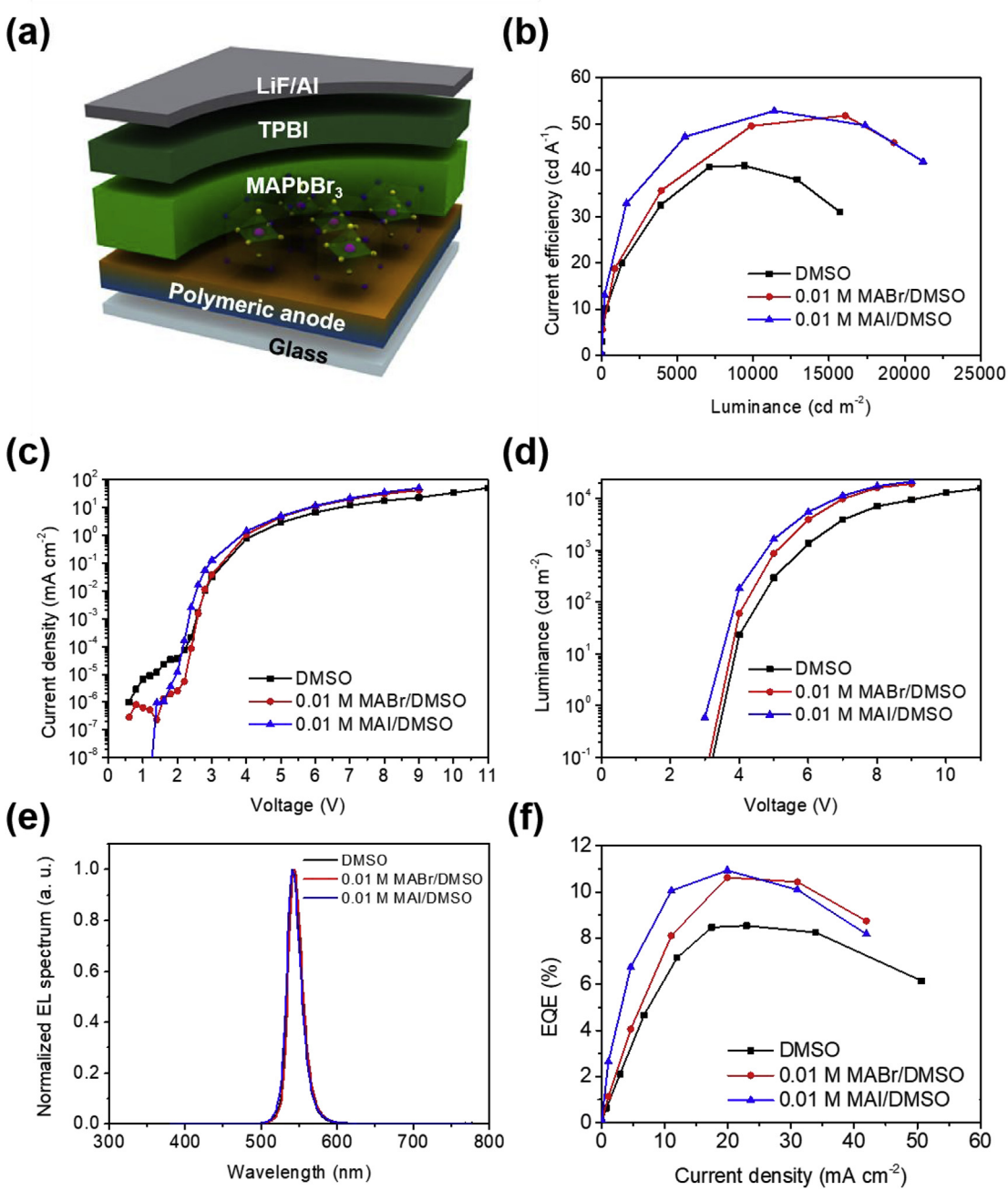

Fig. 5. (a) Schematic device structure of green PeLED on top of polymeric anode. (b) Current efficiency, (c) current density, (d) luminance, (e) EL spectrum and, (f) EQE of green PeLED on top of HWFPAs with different additives. (For interpretation of the references to colour in this figure legend, the reader is referred to the Web version of this article.)

lifetime of devices increased (~1.6 h for DMSO, ~3.2 h for MABr/DMSO and ~5.0 h for MAI/DMSO). The decreased overshoot and prolonged lifetime can be attributed to lowered operating voltages of PeLEDs. It has been reported that the overshoot in the luminance-time curves of PeLEDs is caused by ion migration in MHP layers during operation, causing instability in PeLEDs [45]. The lowered operating voltages can alleviate the ion migration and result in decreased overshoot and increased lifetime.

In PeLEDs, the device efficiency tends to increase as the operating voltage increases [46]. Therefore, decreasing the operating voltage by increasing the κ of the CPA enables the device to survive at high voltage and to have increased maximum device efficiency. To determine whether the increased efficiency of PeLEDs with MABr/DMSO and MAI/DMSO additives could be caused by a factor other than the increase in κ, we quantified the photoluminescence (PL) lifetime (Fig. S9; Table S7). The $MAPbBr_3$ on top of the HWFPA with the DMSO, MABr/DMSO and MAI/DMSO showed similar PL lifetime despite the increased κ. The composition of the underlying anodes did not affect the XRD patterns, and the MABr and MAI in the HWFPA did not affect the crystallinity of the $MAPbBr_3$ layer (Fig. S10). Also, the scanning electron microscope (SEM) images of the $MAPbBr_3$ layers on top of the CPAs did not show any big difference in the morphologies depending on the additives in the CPAs (Fig. S11). Therefore, we attributed the improved maximum efficiency in PeLEDs to the increase in κ that was caused by the MABr/DMSO and MAI/DMSO additives.

4. Conclusion

In this study, we developed ideal CPA with the effective co-additive system to increase the κ, *WF*, and blocking capability of exciton quenching; use of this CPA yielded highly-efficient polycrystalline PeLEDs that operate at low voltages. The new co-additive was composed of organic polar solvents, organic ammonium halide salts, and PFI; use of the DMSO/MAI additive increased κ to $1408.47 \pm 116.77\ \mathrm{S\,cm^{-1}}$, which is currently the highest among additive-incorporated PEDOT:PSS films without post-treatments on the films. The increased κ was attributed to reduced π-π stacking distance, to change in the preferred resonance structure from benzoid to quinoid in conducting PEDOT chains, and to the change of PEDOT chain conformation from coiled to linear. Use of the co-additive (DMSO/MAI/PFI) to make the HWFPA increased its κ without any loss of *WF* due to the effective decoupling of *WF* with the κ. The high κ of anodes in the PeLEDs increased their CE_{max}. The HWFPA with only DMSO had $CE_{max} = 41.01\ \mathrm{cd\,A^{-1}}$, whereas the HWFPA with added MABr/DMSO had $CE_{max} = 51.82\ \mathrm{cd\,A^{-1}}$, and the HWFPA with added MAI/DMSO had $CE_{max} = 52.86\ \mathrm{cd\,A^{-1}}$. This use of co-additive without post-treatments may increase the possibility that PEDOT:PSS anodes can be developed for the industrial applications.

Acknowledgements

This research was supported by the Nano Material Technology Development Program through the National Research Foundation of Korea funded by the Ministry of Science and Innovation, New Zealand (NRF-2014M3A7B4051747). Also, this work was supported by the National Research Foundation of Korea grant funded by the Korea government (Ministry of Science and ICT) (NRF-2016R1A3B1908431). This research was also supported by Creative Materials Discovery Program through the National Research Foundation of Korea funded by Ministry of Science and Innovation, New Zealand (NRF-2018M3D1A1058536).

Appendix A. Supplementary data

Supplementary data to this article can be found online at https://doi.org/10.1016/j.nanoen.2019.03.030.

References

[1] Y. Ling, Z. Yuan, Y. Tian, X. Wang, J.C. Wang, Y. Xin, K. Hanson, B. Ma, H. Gao, Adv. Mater. 28 (2016) 305–311.
[2] L. Zhang, X. Yang, Q. Jiang, P. Wang, Z. Yin, X. Zhang, H. Tan, Y.M. Yang, M. Wei, B.R. Sutherland, E.H. Sargent, J. You, Nat. Commun. 8 (2017) 15640.
[3] Z. Chen, C. Zhang, X. Jiang, M. Liu, R. Xia, T. Shi, Adv. Mater. 29 (2017) 1603157.
[4] H.-K. Seo, H. Kim, J. Lee, M.-H. Park, S.-H. Jeong, Y.-H. Kim, S.-J. Kwon, T.-H. Han, S. Yoo, T.-W. Lee, Adv. Mater. 29 (2017) 1605587.
[5] Z. Yu, X. Niu, Z. Liu, Q. Pei, Adv. Mater. 23 (2011) 3989–3994.
[6] M. Vosgueritchian, D.J. Lipomi, Z. Bao, Adv. Funct. Mater. 22 (2012) 421–428.
[7] M.S. White, M. Kaltenbrunner, E.D. Głowacki, K. Gutnichenko, G. Kettlgruber, I. Graz, S. Aazou, C. Ulbricht, D.A.M. Egbe, M.C. Miron, Z. Major, M.C. Scharber, T. Sekitani, T. Someya, S. Bauer, N.S. Sariciftci, Nat. Photon. 7 (2013) 811–816.
[8] J.Y. Oh, S. Kim, H. Baik, U. Jeong, Adv. Mater. 28 (2016) 4455–4461.
[9] S. Jeong, S. Woo, T. Han, M. Park, H. Cho, Y. Kim, H. Cho, H. Kim, S. Yoo, T.-W. Lee, NPG Asia Mater. 9 (2017) e411.
[10] Y.H. Kim, H. Cho, J.H. Heo, T.S. Kim, N. Myoung, C.L. Lee, S.H. Im, T.-W. Lee, Adv. Mater. 27 (2015) 1248–1254.
[11] H. Cho, S.-H. Jeong, M.-H. Park, Y.-H. Kim, C. Wolf, C.-L. Lee, J.H. Heo, A. Sadhanala, N. Myoung, S. Yoo, S.H. Im, R.H. Friend, T.-W. Lee, Science 350 (2015) 1222–1225.
[12] H. Cho, C. Wolf, J.S. Kim, H.J. Yun, J.S. Bae, H. Kim, J. Heo, S. Ahn, T.-W. Lee, Adv. Mater. 29 (2017) 1700579.
[13] Y.-H. Kim, C. Wolf, Y.-T. Kim, H. Cho, W. Kwon, S. Do, A. Sadhanala, C.G. Park, S. Rhee, S.H. Im, R.H. Friend, T.-W. Lee, ACS Nano 11 (2017) 6586–6593.
[14] Y.-H. Kim, G.-H. Lee, Y.-T. Kim, C. Wolf, H.J. Yun, W. Kwon, C.G. Park, T.-W. Lee, Nanomater. Energy 38 (2017) 51–58.
[15] M. Vosgueritchian, D.J. Lipomi, Z. Bao, Adv. Funct. Mater. 22 (2012) 421–428.
[16] A.M. Nardes, M. Kemerink, M.M. De Kok, E. Vinken, K. Maturova, R.A.J. Janssen, Org. Electron. 9 (2008) 727–734.
[17] J. Liu, X. Wang, D. Li, N.E. Coates, R.A. Segalman, D.G. Cahill, Macrocmolecules 48 (2015) 585–591.
[18] I. Lee, G.W. Kim, M. Yang, T. Kim, ACS Appl. Mater. Interfaces 8 (2016) 302–310.
[19] C.M. Palumbiny, C. Heller, C.J. Scha, V. Ko, G. Santoro, S. V Roth, P. Mu, J. Phys. Chem. C 118 (2014) 13598–13606.
[20] N. Kim, B.H. Lee, D. Choi, G. Kim, H. Kim, J.-R. Kim, J. Lee, Y.H. Kahng, K. Lee, Phys. Rev. Lett. 109 (2012) 106405.
[21] Y.H. Kim, C. Sachse, M.L. Machala, C. May, L. Müller-meskamp, K. Leo, Adv. Funct. Mater. 21 (2011) 1076–1081.
[22] W. Zhang, B. Zhao, Z. He, X. Zhao, H. Wang, S. Yang, H. Wu, Y. Cao, HEnergy Environ. Sci. 6 (2013) 1956–1964.
[23] N. Kim, H. Kang, J.H. Lee, S. Kee, S.H. Lee, K. Lee, Adv. Mater. 27 (2015) 2317–2323.
[24] Y. Xia, K. Sun, J. Ouyang, Adv. Mater. 24 (2012) 2436–2440.
[25] Y. Xia, K. Sun, J. Ouyang, Energy Environ. Sci. 5 (2012) 5325–5332.
[26] B.J. Worfolk, S.C. Andrews, S. Park, J. Reinspach, N. Liu, M.F. Toney, S.C.B. Mannsfeld, Z. Bao, Proc. Natl. Acad. Sci. U. S. A 112 (2015) 14138–14143.
[27] M. Cai, Z. Ye, T. Xiao, R. Liu, Y. Chen, R.W. Mayer, R. Biswas, K. Ho, R. Shinar, J. Shinar, Adv. Mater. 24 (2012) 4337–4342.
[28] Y. Chih, J. Wang, R. Yang, C. Liu, Y. Chang, Y. Fu, W. Lai, P. Chen, T. Wen, Y. Huang, C. Tsao, Adv. Mater. 28 (2016) 8687–8694.
[29] Z.-K. Tan, R.S. Moghaddam, M.L. Lai, P. Docampo, R. Higler, F. Deschler, M. Price, A. Sadhanala, L.M. Pazos, D. Credgington, F. Hanusch, T. Bein, H.J. Snaith, R.H. Friend, Nat. Nanotechnol. 9 (2014) 687–692.
[30] B.R. Lee, S. Lee, J.H. Park, E.D. Jung, J.C. Yu, Y.S. Nam, J. Heo, J.Y. Kim, B.S. Kim, M.H. Song, Adv. Mater. 27 (2015) 3553–3559.
[31] Y.-H. Kim, C. Wolf, H. Kim, T.-W. Lee, Nanomater. Energy 52 (2018) 329–335.
[32] Y.-H. Kim, S. Kim, S.H. Jo, T.-W. Lee, Small Methods 2 (2018) 1800093.
[33] J. Byun, H. Cho, C. Wolf, M. Jang, A. Sadhanala, R.H. Friend, H. Yang, T.-W. Lee, Adv. Mater. 28 (2016) 7515–7520.
[34] K. Tanaka, T. Takahashi, T. Ban, T. Kondo, K. Uchida, N. Miura, Solid State Commun. 127 (2003) 619–623.
[35] T.-W. Lee, Y. Chung, Adv. Funct. Mater. 18 (2008) 2246–2252.
[36] N. Naujoks, J. Dual, B.U. Lang, E. Mu, Adv. Funct. Mater. 19 (2009) 1215–1220.
[37] L. Ouyang, C. Musumeci, M.J. Jafari, T. Ederth, ACS Appl. Mater. Interfaces 7 (2015) 19764–19773.
[38] S. Garreau, J.L. Duvail, G. Louarn, Synth. Met. 125 (2002) 325–329.
[39] T. Chou, S. Chen, Y. Chiang, Y. Lin, C. Chao, J. Mater. Chem. C. 3 (2015) 3760–3766.
[40] B.J. Ouyang, C. Chu, F. Chen, Q. Xu, Y. Yang, Adv. Funct. Mater. 15 (2005) 203–208.
[41] J. Ouyang, Q. Xu, C. Chu, Y. Yang, G. Li, J. Shinar, Polymer 45 (2004) 8443–8450.
[42] Z. Yu, Y. Xia, D. Du, J. Ouyang, ACS Appl. Mater. Interfaces 8 (2016) 11629.
[43] Y. Xia, K. Sun, J. Ouyang, J. Mater. Chem. 3 (2015) 15897–15904.
[44] Z. Yu, Y. Xia, D. Du, J. Ouyang, ACS Appl. Mater. Interfaces 8 (2016) 11629.
[45] H. Cho, Y.-H. Kim, C. Wolf, H.-D. Lee, T.-W. Lee, Adv. Mater. (2018) 1704587.
[46] L. Zhao, J. Gao, Y.L. Lin, Y. Yeh, K.M. Lee, N. Yao, Y. Loo, B.P. Rand, Adv. Mater. 29 (2017) 1605317.

Su-Hun Jeong received his B.S. (2012) and Ph.D (2017) in Materials Science and Engineering from Pohang University of Science and Technology (POSTECH), Korea. He is currently working in Materials Science and Engineering at Seoul National University, Korea as a postdoctoral researcher. His current research work is focused on polymeric electrodes for flexible organic and perovskite optoelectronic devices.

Hobeom Kim received his Ph.D. (2017) in the Department of Materials Science and Engineering at Pohang University of Science and Technology (POSTECH), Korea. After his postdoc in Seoul National University (SNU) (2017–2018), Korea, he is currently working in Group for Molecular Engineering of Functional Materials (GMF), Ecole polytechnique fédérale de Lausanne (EPFL), Swiss as a postdoctoral researcher (2018-). His research activity has been focused on optoelectronic devices such as solar cells and light-emitting diodes with organic and perovskite materials.

Min-Ho Park received his M.S. (2013) and Ph.D (2017) in Materials Science and Engineering from Pohang University of Science and Technology (POSTECH), Korea and his B. S. (2011) in department of Material Science and Engineering from Inha University, Korea. He is currently working in Materials Science and Engineering at Seoul National University, Korea as a postdoctoral researcher. His research interests include vacuum- or solution-processed light-emitting diodes by using the organic or organic-inorganic perovskite materials for displays and solid-state lightings.

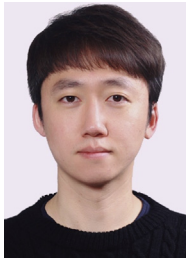

Yeongjun Lee is a postdoctoral researcher in Materials Science and Engineering at Seoul National University, Korea. He received his M.S. (2014) and Ph.D. (2018) in Materials Science and Engineering from Pohang University of Science and Technology (POSTECH), Korea. His research interests include printed electronics, nanowire electronics, stretchable polymer electronics, and organic neuromorphic electronics.

Nannan Li is a postdoctoral research scientist in School of Natural Sciences at Ulsan National Institute of Science and Technology (UNIST), Republic of Korea. She obtained her Ph.D. degree in Physics department from Pohang University of Science and Technology (POSTECH) in 2015. Since then she works as a postdoctoral researcher in Center for Superfunction Materials, UNIST. Her research work mainly focuses on the density function theory (DFT) calculation of low dimensional nanomaterials and their related applications. She is not only working on carbon materials such as graphene and carbon nanotubes, but also on transition metal dichalcogenides and their hetero-nanomaterials.

Hong-Kyu Seo received his Ph.D. (2017) in Division of Environmental Science and Engineering from Pohang University of Science and Technology (POSTECH), Korea. He is currently working in Samsung Advanced Institute of Technology (SAIT), Korea as a senior researcher. His research focuses on graphene electronics and organic-inorganic hybrid materials for flexible displays and solid-state lightings.

Tae-Hee Han received his B.S. (2010) and Ph.D. (2015) in Materials Science and Engineering from Pohang University of Science and Technology (POSTECH), Republic of Korea. He is currently a postdoctoral researcher in Prof. Yang Yang's group in University of California Los Angeles (UCLA) since 2017. His research focuses on organic and organic/inorganic hybrid materials for optoelectronic applications, such as photovoltaic cells, and light-emitting diodes.

Soyeong Ahn is currently a Ph.D candidate in Materials Science and Engineering at Pohang University of Science and Technology (POSTECH), Korea. She received her M.S. and B.S degrees in Chemical Engineering from Kyung Hee University in February 2015. Her current research focuses on solution-processed electronics based on organic and organic-inorganic hybrid materials for flexible displays, solid-state lightings, and solar energy devices.

Jung-Min Heo received his B.S. in School of Advanced Materials Science and Engineering in 2016 from Sungkyunkwan University (SKKU), Korea. He is graduate student in Seoul National University (SNU), Korea since 2017. His current research work is focused on organic-inorganic hybrid perovskite optoelectronics and photophysics in semiconducting materials and electronic devices.

Kwang S. Kim received his Ph.D. degree from University of California, Berkeley. He was a postdoctoral fellow at IBM and a visiting professor or scientist at Rutgers University, MIT, and Columbia University. He was a professor in Department of Chemistry, Pohang University of Science and Technology. Currently, he is a distinguished professor in Department of Chemistry and the director of the Center for Superfunctional Materials at Ulsan National Institute of Science and Technology (UNIST). His research interest includes theoretical and experimental nanoscience centered on novel nanomaterials and nanodevices.

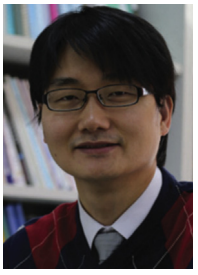

Tae-Woo Lee is a professor in Materials Science and Engineering at Seoul National University, Korea. He received his Ph.D in Chemical Engineering from KAIST, Korea in 2002. He joined Bell Laboratories, USA as a postdoctoral researcher and worked at Samsung Advanced Institute of Technology as a member of research staff (2003–2008). He was an associate professor in Materials Science and Engineering at Pohang University of Science and Technology (POSTECH), Korea until August 2016. His research focuses on organic, organic-inorganic hybrid perovskite and carbon materials, and their applications to flexible electronics, printed electronics, displays, solid-state lightings, solar energy conversion devices, and bio-inspired neuromorphic devices.